COMMUNICATION

Highly Stretchable, Strain Sensing Hydrogel Optical Fibers

Jingjing Guo, Xinyue Liu, Nan Jiang, Ali K. Yetisen, Hyunwoo Yuk, Changxi Yang, Ali Khademhosseini, Xuanhe Zhao, and Seok-Hyun Yun*

Hydrogels are widely used in tissue engineering,[1] drug delivery,[2] and wound dressings.[3] Recently, efforts have been made to integrate photonic functions into hydrogel materials for novel biomedical applications, including functional optical fibers for light delivery and monitoring of blood oxygenation levels in biological tissues,[4] cell-containing hydrogel implants for toxicity sensing and optogenetic therapy,[5] and nanoparticle-embedded hydrogels for detection of biochemical analytes.[6] However, due to the weak and brittle nature of common synthetic hydrogels,[7] these hydrogel photonic devices are relatively fragile against external stress and strain. The low mechanical strength poses a practical challenge for these hydrogels' applications in wearable or implantable devices because the body motion and tissue movement may degrade or damage the structure and function.[8] A number of recipes for polymer gels to obtain mechanical toughness, resilience, and elasticity, as well as flexibility have been demonstrated.[9,10] One of the most promising approaches is to form a hybrid of ionic and covalent polymer networks where the covalently crosslinked long-chain polymers give high stretchability of the hydrogel and the reconfigurable ionically crosslinked polymers enhance the hydrogel's toughness by dissipating mechanical energy under deformation.[11] The hybrid network of ionically crosslinked alginate and covalently crosslinked polyacrylamide has shown remarkable stretching capability, high fracture energy of ~9000 J m^{-2},[11] and biocompatibility.[7,12] Despite recent enhancements of hydrogels' mechanical properties, highly stretchable and robust hydrogel photonic devices have not been achieved yet.

Here, we report the design and fabrication of highly stretchable and tough optical fibers made of optically optimized alginate-polyacrylamide hydrogel materials in a core/clad step-index structure (Figure S1, Supporting Information). The fibers can be elongated to an axial strain of 700% and then relaxed over multiple cycles. Functional molecules, such as organic dyes, may also be incorporated into the porous matrix of hydrogels by solution doping. Harnessing these unique properties, we have devised a novel, simple technique for measuring axial strain and accomplished distributed strain sensing based on dye-doped hydrogel fibers with a large dynamic strain range.

Light guiding is achieved by total internal reflection at the interface between the core and clad, for which the refractive index of the core should be larger than that of the clad. We characterized the optical properties of alginate-polyacrylamide hydrogels made with different concentration of acrylamide (AAm) in precursor solution. The concentration of alginate (solubility: <4 wt%) was fixed at 2 wt% optimal for high fracture energy.[11] Samples were fabricated by polymerization and crosslinking of alginate-polyacrylamide precursor solution under UV irradiation. The optical attenuation spectra of the samples in cuvettes showed optical loss increasing with acrylamide concentration (Figure S2, Supporting Information). For AAm concentrations below 40 wt%, hydrogels formed in cuvettes exhibited high transparency, and the average losses in the visible range (400–700 nm) were less than 0.4 dB cm^{-1} (**Figure** 1a). The refractive indices of hydrogels are higher than those of precursor solutions because of the densification of polymer chains after crosslinking (Figure 1b).

To characterize the swelling properties, hydrogels were fabricated at different AAm concentrations, and their weights were measured immediately after crosslinking (pre-swelling state) and later after they have been immersed in Dulbecco's Modified Eagle Medium (DMEM) at 37 °C and 5% CO_2 for 3 d. The weights of postswelling samples increased by a factor of 1.53–1.62 with respect to the preswelling states (Figure 1c), almost independent of the AAM concentration. The nearly constant expansion ratio is desirable for composite fibers because the core and clad hydrogels would expand to the same degree. The swelling ratio, which is defined as the weight ratio with respect to its dried mass, were measured to decrease in proportion to the inverse of the AAm concentration (Figure 1c), which is expected from different shear modulus increasing with

J. Guo, Dr. A. K. Yetisen, Prof. S.-H. Yun
Harvard Medical School and Wellman Center
for Photomedicine
Massachusetts General Hospital
65 Landsdowne Street, Cambridge
Massachusetts 02139, USA
E-mail: syun@hms.harvard.edu
J. Guo, Prof. C. Yang
State Key Laboratory of Precision Measurement
Technology and Instruments
Department of Precision Instruments
Tsinghua University
Beijing 100084, China
X. Liu, H. Yuk, Prof. X. Zhao
Soft Active Materials Laboratory
Department of Mechanical Engineering
Massachusetts Institute of Technology
Cambridge, MA 02139, USA
Dr. N. Jiang, Prof. A. Khademhosseini
Biomaterials Innovation Research Center
Engineering in Medicine Division
Brigham and Women's Hospital
Harvard Medical School
Cambridge, MA 02139, USA
Dr. N. Jiang
State Key Laboratory of Advanced Technology
for Materials Synthesis and Processing
Wuhan University of Technology
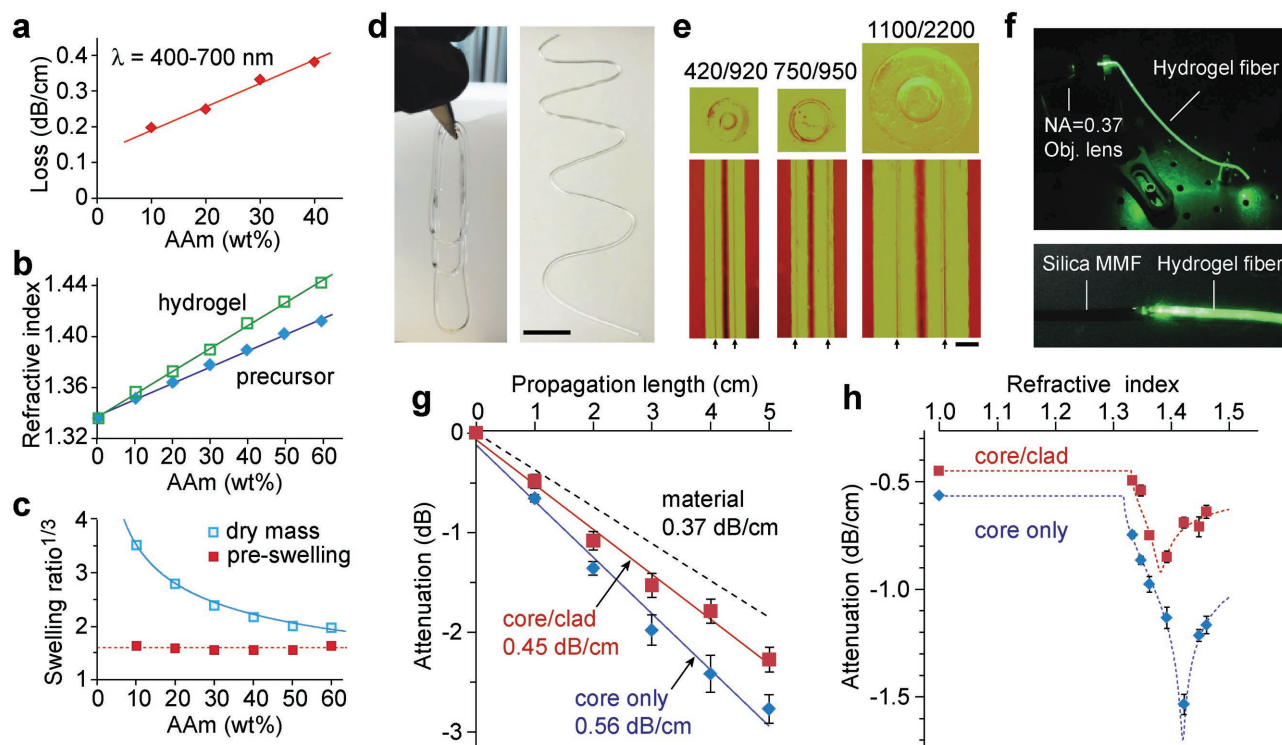122, Luoshi Road, Wuhan 430070, China

Figure 1. Optical properties of step-index, core/clad alginate-polyacrylamide hydrogel fibers. a) The dependence of optical attenuation in hydrogels on the acrylamide (AAm) concentration, averaged over the visible spectrum (400–700 nm). b) The refractive index of alginate-polyacrylamide precursors (solid diamonds) and crosslinked hydrogels (open squares) as a function of the concentration of acrylamide. c) Linear expansion ratio, determined from the cube root (red squares) of the measured weight ratio between a fully swollen state and immediately after fabrication (pre-swelling) or the cube root (cyan squares) of the swelling ratio between fully swollen samples and dry mass. Dotted lines: curve fits based on a linear line (magenta) or $y = A/x$, where A is constant (cyan). d) Photos of fabricated hydrogel fibers. Scale bar, 1 cm. e) Phase-contrast images of three hydrogel fibers in deionized water. Arrows indicate the interface between the core and clad; the numbers indicate the core and cladding diameters (420/920 means 420 µm-diameter core and 920 µm clad). Scale bar, 500 µm. f) Photos showing 532 nm laser light guided through and scattered from a hydrogel fiber (top) and a hydrogel fiber connected to a multimode silica fiber (core diameter: 100 µm; NA = 0.37) (bottom). g) Propagation loss of pre-swelling hydrogel fibers in air with/without cladding, measured by a cutback technique. h) Propagation loss of pre-swelling hydrogel fibers as a function of external refractive index. Symbols, experimental data. Lines, curve fits based on the Fresnel Equation. Error bars, s.d. ($n = 3$) in (g) and (h).

polymer concentration. We chose 40 wt% AAm concentration for the core and 20 wt% for the clad. In this case, the numerical aperture of a preswelling step-index fiber (NA $= \sqrt{n_{co}^2 - n_{cl}^2}$) would be 0.325, where n_{co} is the core index (≈ 1.411) and n_{cl} is the clad index (≈ 1.373). At a fully swollen state, the effective acrylamide concentrations in the core and clad would be reduced to 5.2% and 11.2%, and the refractive index decrease to ≈ 1.3545 and 1.3494, respectively, and NA is reduced to 0.117.

We developed a series of steps to fabricate the core–clad fibers (Figure S3, Supporting Information). First, the core was fabricated by injecting a Ca^{2+}-containing alginate-polyacrylamide precursor solution into a platinum-cured silicone tube mold with a syringe and curing the solution by UV light irradiation. After polymerization, the core was extracted from the mold by swelling the tube in dichloromethane for 20 min. Next, the clad was formed on the core fiber by a two-step dip-coating method. The ionic cross-linking of alginate chains by Ca^{2+} results in high viscosity and makes it hard to dip the core and coat a cladding layer on it. To solve this problem, the core was first dipped in Na^+-containing alginate-polyacrylamide precursor and polymerized under UV light to form a layer of Na-alginate-polyacrylamide hydrogel that consists of covalently

cross-linked polyacrylamide chains and well-dispersed, but not yet cross-linked, alginate chains.[13] To achieve robust bonding between the core and clad, we chemically anchored the alginate on the core via EDC-NHS chemistry.[12,14] Then, the fiber was immersed in an aqueous solution of $CaCl_2$ to complete Ca^{2+}-mediated ionic cross-linking of alginate in the clad. The fabricated hydrogel fiber exhibited excellent mechanical flexibility (Figure 1d).

Using various tube molds of different inner diameters and varying the clad dipping time, hydrogel fibers with various core and clad diameters were fabricated. The diameter of the crosslinked core when taken out of the mold is identical to the inner diameter of the mold (pre-swelling), but it increases by a factor of 1.5–1.7 at fully swollen states (Figure S4, Supporting Information). When tube diameters were 250, 500, and 750 µm, respectively, the core diameters were 420, 750, and 1100 µm in the core-clad fibers that have been fully swollen in deionized water (Figure 1e). The thickness of the clad layer is controlled by the dipping time and can be thin (<50 µm) or thick (>500 µm).

Light guiding was confirmed by launching a laser beam into the core (Figure 1f). It was possible to splice the hydrogel

fibers with conventional silica-based multimode fibers by physically inserting a thin but stiff silica fiber into the hydrogel fiber. Alternatively, the short section of a pigtail silica fiber was embedded in the core precursor solution in the mold prior to crosslinking, and subsequent UV polymerization and cladding coating formed a smooth, low-loss connection (Figure 1f). The propagation loss of various hydrogel fibers was measured by using a cutback technique (see the Experimental Section for details).[15] The optical loss increased exponentially (linearly in dB scale) with the fiber length (Figure 1g). The measured loss coefficient of the core/clad hydrogel fibers (750/1100 µm) in air was 0.45 dB cm^{-1} at a wavelength (λ) of 532 nm, which was close to the material loss of the core (0.37 dB cm^{-1}). We also measured the loss of core-only fibers (750 µm) without adding cladding layers and measured an only modestly higher loss of 0.56 dB cm^{-1}. The core-only fibers guide light effectively via the total internal reflection at the hydrogel-air interface. However, this core-only guiding mechanism is fragile in high refractive-index environments.

To investigate the dependence on the refractive index of the surrounding medium,[16] we used a mixture of glycerol and deionized water with different ratios. For core-only fibers, light guiding relies on the reflection at the interface of the core and surrounding medium, which decreases to zero in principle when their refractive indices are matched. Our measurements showed significant increases of the propagation loss when the external refractive index was closer to the core refractive index (Figure 1h). The measured data were fit reasonably well with a curve obtained with the Fresnel equation with an incidence angle as a fitting parameter.[17] The core-clad fibers had overall lower losses (Figure 1h). However, they also exhibited some sensitivity to the surrounding medium, which is not expected in a perfect lossless step-index fiber. This dependence to the surrounding index is attributed to the light that is leaked from the core but guided in the clad layer, which otherwise could contribute to the transmission but was extracted out by index matching to the surrounding medium.

Hydrogel fibers exhibited excellent elastic stretchability in both pre- and post-swelling states (**Figure 2**a) and were stretchable repeatedly without apparent plastic deformations (Figure 2b). Optical microscopy images of fibers revealed some spatial inhomogeneity in the fiber, which became more apparent in stretched fibers (Figure 2c). This wrinkle pattern, presumably related to the inhomogeneous distribution of crosslink density,[18] is thought to contribute to the waveguide loss. The mechanical properties of the fibers were measured with an Instron analyzer in the tensile mode. A mm-diameter hydrogel fiber (750/1100 µm), for example, showed a Young's modulus of ≈80 kPa, large elongation up to 730%, and a high failure stress of 230 kPa (Figure 2d). The rupture strain value is lower than previously reported values (≈2000%) for alginate-polyacrylamide hydrogels made with lower acrylamide concentrations (<14 wt%).[11] With increasing concentration (20–40 wt%), the hydrogel matrix tends to be more rigid and less stretchable.

Recently, there have been heightened interests in flexible, stretchable and biocompatible sensors for health monitoring and human-machine interfacing.[19–21] Strain sensing has applications to human motion detection,[22] skin-like sensing devices,[23] and posture and biomechanics analysis.[24] In biomechanical settings, strain measurement is commonly based on piezoresistive effects. A number of conductive materials such as carbon nanotubes[22,25] and hybrid composites[26,27] have been investigated as sensing elements for high sensitivity and precision. However, for biomedical miniaturization electrical and electromagnetic insulation and the biocompatibility of metallic components pose practical challenges.[28] Optical strain sensors, especially fiber-optic sensors, have been studied as an alternative to piezoresistive sensors,[29,30] because of their unique advantages of compact size, inherent electrical safety,
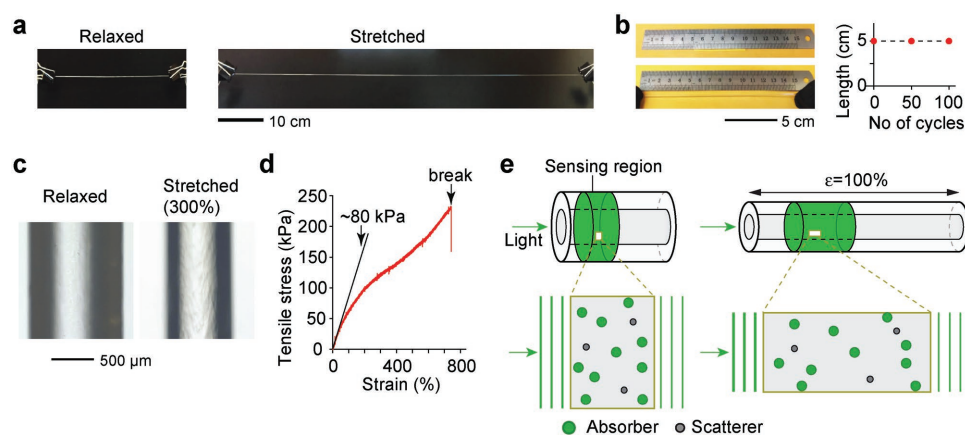

Figure 2. Mechanical properties of alginate-polyacrylamide hydrogel fibers. a) Photos demonstrating 3X stretching of a hydrogel fiber. b) Elasticity of fibers (750/1100 µm) against repeated 3X stretching for core/clad, showing no change in fiber length after 100 cycles. Photos show a 5 cm long fiber in the relaxed state, top, and stretched state, bottom. c) Optical microscope images of light transmission through a hydrogel fiber in the relaxed (left) and stretched (right) conditions. d) A typical stress-strain curve of a fully swollen hydrogel fiber. The slope in the low-strain region gives a Young's modulus of ≈80 kPa. e) Illustration of the optical loss in a sensing region containing absorption and scattering elements. As the fiber is stretched, the distribution of the loss elements is altered, resulting in loss increasing exponentially with the length of the sensing region. This relation offers a simple technique for strain sensing.
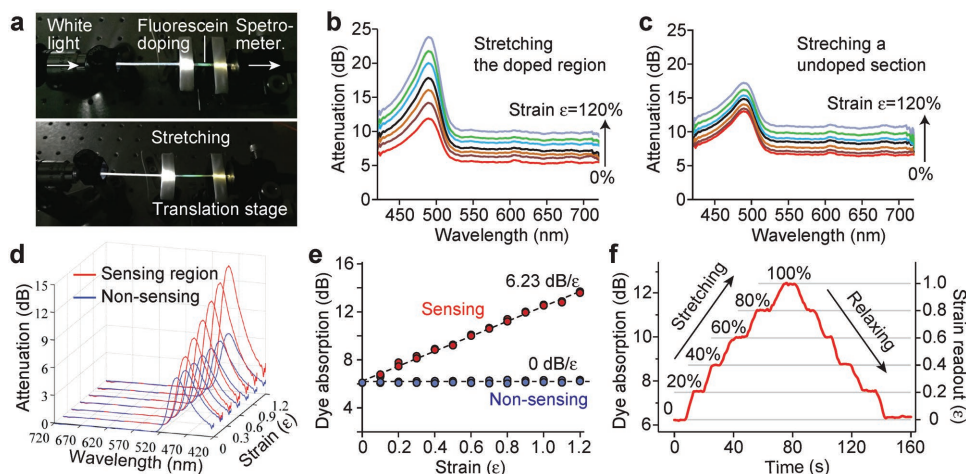
Figure 3. Dye-loaded hydrogel fibers for strain sensing. a) Setup for stretching a section of fiber doped with fluorescein (green region). b) The measured attenuation spectra as the sensing region was stretched. c) The attenuation spectra when the strain was applied to an un-doped section. d) Dye absorption spectra, $a_1(l_1)R_1(\lambda)$, extracted from the attenuation spectra. e) The magnitude of dye absorption at the peak wavelength (480 nm) as a function of strain applied to the sensing (red) and undoped (blue) regions. Data for three repeated measurements are shown. f) Time responses of the fiber sensor with respect to step-tuned strain up to ε_1 of 100%. The strain readout of the sensor is in good agreement with the applied strain values.

immunity to electromagnetic interferences, and multiplexing capacities. Despite the potential of fiber-optic strain sensors for biomechanical applications, the optical fibers, commonly made of glass and plastics,[31] are stiff and hardly stretchable (maximum strain: <1%[32]). Although the conventional silica fibers are widely used for strain measurement and health monitoring of solid engineering constructs and civil structures, such as buildings, dams, and airplanes, they are not well suited to work with soft matters and large strain.

To harness the unique mechanical properties of the fibers we have developed, we devised a novel technique for strain measurement. Consider a section of a fiber containing loss elements, such as absorbing molecules and scattering particles, characterized by specific absorption and scattering cross-sections (Figure 2e). The amount of absorption and scattering is proportional to the product of the number of loss elements in the volume, the cross-sectional areas, and the optical intensity. The Poisson's ratios of polyacrylamide gels was estimated to be ≈0.46,[33] and that of alginate gels is ≈0.5,[34] making the hybrid hydrogels nearly incompressible. As the fiber is elongated, the number of elements, volume of the segment, and cross-sections are unchanged, but the optical intensity is increased as the fiber is stretched and its diameter is reduced. Therefore, the attenuation in dB scale increases linearly with strain. This result is consistent with the Beer–Lambert law,[35] which states that the optical attenuation $S(\lambda,l)$ in a logarithmic (dB) scale is proportional to the fiber length: $I = I^0(1 + \varepsilon)$, where l^0 is the original length and ε is the magnitude of axial strain. Therefore, the magnitude of strain can be determined directly from the measurement of attenuation. To our knowledge, this relationship of loss and strain has not been reported in the context of strain measurement.

We harnessed this principle to demonstrate strain sensing using the highly stretchable, hydrogel fibers. Imagine a fiber where dye molecules with a normalized absorption spectrum, $R_1(\lambda)$, are doped into a short section with a length l^0_1. Assuming the spectral property of each loss mechanism does not change

upon strain, the measured attenuation in the dB scale can be expressed as

$$S(\lambda,l)\,[\mathrm{dB}] = a_0(l)R_0(\lambda) + a_1(l_1)R_1(\lambda) \tag{1}$$

where $a_0(l)$ represents the strain-dependent change of the intrinsic fiber loss characterized by a normalized loss spectrum $R_0(\lambda)$, and $a_1(l_1)$ is a coefficient representing the contribution of dye absorption, which is linearly proportional to the length of the doped region: $l_1 = l^0_1(1 + \varepsilon_1)$, where ε_1 is the strain of the doped region. When $R_0(\lambda) \neq R_1(\lambda)$, the two coefficients $a_1(l)$ and $a_1(l_1)$, can be obtained by minimization of the sum of the squared errors[36]

$$\sum_{i=1}^{N}\left[S(\lambda_i,\varepsilon) - a_1(\varepsilon_1)R_1(\lambda_i) - a_0(\varepsilon)R_0(\lambda_i)\right]^2 \tag{2}$$

The strain ε_1 in the doped region is determined from $\varepsilon_1 = [a_1(l_1) - a_1(l^0_1)]/a_1(l^0_1)$, where we used the relation that the attenuation increases linearly with length.

To verify this principle experimentally, we first measured the strain-dependent intrinsic loss of hydrogel fibers, fully swollen in deionized water, using a white light source and a spectrometer. The measured profile $R_1(\lambda)$ was nearly invariant against strain up to 1.2 (or 120%), and the coefficient $a_0(l)$ indeed showed a linear dependence on the stretched fiber length (Figure S5, Supporting Information). Next, a sensing region was prepared by loading organic dye, fluorescein, via solution doping.[4] Droplets of dye solution (3 μL, 0.01% w/v) were applied to the surface of a hydrogel fiber (750/1100 μm) to form a ≈8 mm long dye-doped region (**Figure 3**a). The dye absorption profile has a peak at $\lambda = 480$ nm (Figure S6, Supporting Information). When the sensing region (dye-doped section) was stretched, the attenuation over the entire visible wavelength increased with strain but with the maximum sensitivity at the peak wavelength of dye absorption (Figure 3b). By comparison, when about the same length of un-doped region was stretched the background scattering-induced loss increased (Figure S5, Supporting Information),

COMMUNICATION

but the contribution of dye absorption to the attenuation did not change (Figure 3c). The scattering loss spectrum is distinct from the dye absorption spectrum and therefore was eliminated by spectral fitting (Figure 3d). The magnitude of dye absorption, $a_1(l_1)$, increased linearly with the strain applied to the sensing region, with a linear slope coefficient of 6.23 dB/ε over a range up to $\varepsilon_1 = 1.2$ (Figure 3e). The application of strain on a non-sensing (un-doped) region had a negligible effect on the measured dye-induced attenuation within a system noise (<0.17 dB over the full strain range) (Figure 3e). The sensor output reproduced the applied strain profile with a strain error of less than ±1% (Figure 3f and Figure S7, Supporting Information). After unloading, the fiber attenuation returned to its initial value within ±1% (Figure S7, Supporting Information). To evaluate long-term stability, the attenuation spectrum was monitored for one hour. Fully swollen fibers in moist environment (provided by a humidifier) typically showed a low drift of less than ±1% in strain (Figure S8, Supporting Information). By contrast, initially fully swollen fibers exposed to the laboratory air without a humidifier suffered from considerable strain errors because of the shrinkage of the sensing region (Figure S8, Supporting Information).

We next explored the feasibility of wavelength-division multiplexing (WDM) of multiple sensing regions (**Figure 4**a). Three different dyes were chosen with different absorption spectra: fluorescein (FL, peak wavelength at 488 nm), rhodamine B (RB, peak at 551 nm), and methylene blue (MB, peak at 666 nm). The three dyes were loaded into three discrete locations of a fiber (Figure 4b). Each dye-doped sensor region was 8–10 mm long. The attenuation spectrum of the multiplexed sensor can be expressed as: $S(\lambda, l) = \sum_{i=0}^{3} a_i(l_i) R_i(\lambda)$ or $S = a.R$, where $R_{1,2,3}(\lambda)$ are the reference absorption spectra of the three dyes, respectively (Figure S6, Supporting Information). From the measured attenuation spectrum (Figure S9, Supporting Information), the coefficients, $a_{1,2,3}(l)$, of individual sensors were determined. Each sensor responded to the strain applied to the particular sensor but not to the strain applied to other sensing regions (Figure 4c), with linear slope efficiencies (Figure 4d).

In conclusion, we have demonstrated highly stretchable, elastic fibers made of alginate-polyacrylamide hydrogels in a step-index core/clad structure. The propagation loss of 0.45 dB cm^{-1} in the air was primarily due to the material loss of 0.37 dB cm^{-1}, which may be improved by material optimizations. Using the unique physical and optical properties of the fibers, we demonstrated a novel principle for strain sensing with a large dynamic strain range of 120% and distributed strain sensing based on multiplexing different absorption materials. The strain accuracy was ±1% in short- and long-term measurements in the moist environment, but the readout was sensitive to the variation of swelling state of the hydrogels. The hydrogel fibers may be a useful building block for wearable sensors and implantable therapy-enabling devices, especially when high flexibility, stretchability, and biocompatibility are required.

Experimental Methods

Fabrication of Tough Hydrogel Fibers: The precursor for the core was synthesized by mixing aqueous solutions of 40 wt% acrylamide (AAm; Sigma-Aldrich), 2 wt% sodium alginate (Sigma-Aldrich), 0.06 wt% *N,N*-methylenebisacrylamide (MBAA; Sigma-Aldrich), and 0.16 wt% ammonium persulphate (APS; Sigma-Aldrich) with calcium sulfate (CaSO$_4$, 0.26 wt%; Sigma-Alginate) and *N,N,N′,N′*-tetramethylethylenediamine (TEMED, 0.1% v/v; Sigma-Aldrich). The precursor was injected in a silicone tube mold (inner diameter: 250–1000 μm, Cole Parmer) using a syringe and was crosslinked in nitrogen at 50 °C under ultraviolet irradiation (365 nm, 5 mW cm^{-2}) for 30 min. The tube mold was swelled in dichloromethane for 20 min, and the core hydrogel was extracted. The core fiber was dipped in an Na-alginate-polyacrylamide precursor composed of 20 wt% AAm, 2 wt% alginate, 0.03 wt% MBAA, 0.16 wt% APS, 0.1% v/v TEMED in MES buffer (pH 6.0). EDC/Sulfo-NHS (EDC, Sigma-Aldrich: molar ratio of 25:1 to alginate; Sulfo-NHS, Sigma-Aldrich: molar ratio of 30:1 to alginate) was also added to the solution, which induces robust chemical bonding to the core matrix via EDC-NHS chemistry.[12,14] The clad-coated core fiber hang vertically and cured by UV irradiation for 30 min. After polymerization, the hydrogel fiber with chemically bonded Na-alginate-polyacrylamide clad was immersed in an aqueous solution of CaCl$_2$ (0.1 M; Sigma-Aldrich), for Ca^2-induced crosslinking of alginate chains.
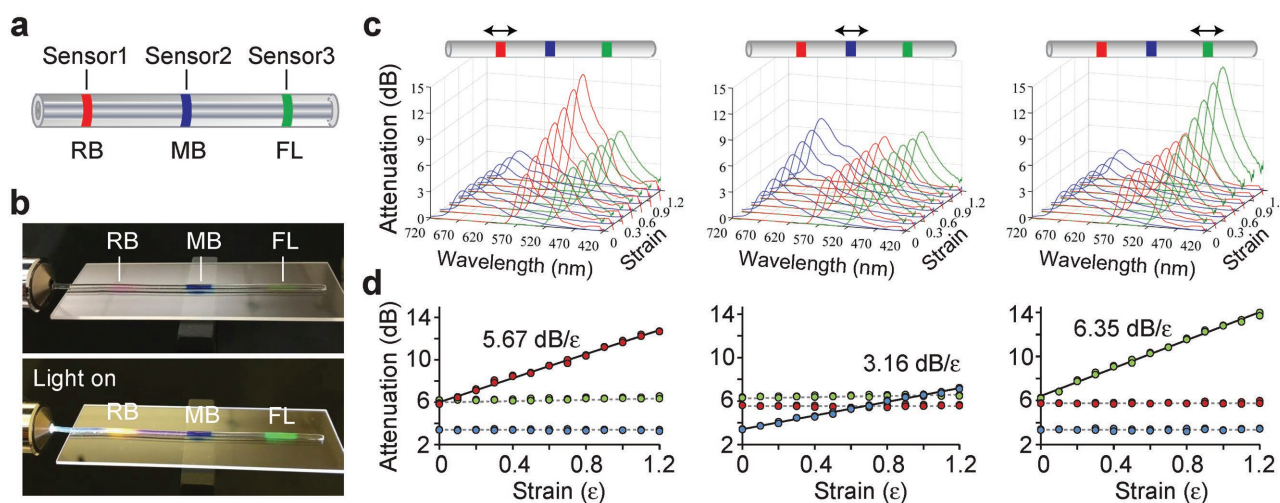

Figure 4. Multiplexed strain sensing. a) Schematic of a fiber with three sensor regions doped with different dyes, respectively: RB: rose Bengal, MB: methylene blue, FL: fluorescein. b) Photos showing a dye-doped fiber on a glass slide, without (top) and with (bottom) excitation broadband light. c) Extracted absorption spectra of the three sensors when local strain was applied to each sensor at a time. d) The dye absorption as a function of strain, showing linear readout in terms of dB/strain and negligible crosstalk between sensors.

Characterization of Alginate-Polyacrylamide Hydrogels: Hydrogels were prepared in standard 1 cm wide poly(methyl methacrylate) disposable cuvettes, and optical attenuation of the hydrogels was measured using a scanning UV–vis spectrometer. The refractive-index measurement was performed at room temperature by using a digital refractometer (Sper Scientific) with a built-in red light source. 100 µL of the precursor were placed on the prism of the refractometer and measured before and after crosslinking under UV irradiation. For swelling test, hydrogels were immersed in DMEM (Gibco Life Technologies), 37 °C, 5% CO_2 environment for 3 d. The swelling ratio (*S*) referring to dried weight was calculated as[37] $S = (W_s - W_d)/W_d$, where W_s and W_d are the measured weights of fully swollen and dried samples, respectively.

Measurement of Light Guiding Loss: The propagation loss of a hydrogel fiber in air was measured by a cutback technique. Laser light at 532 nm was coupled into a hydrogel fiber (750/1100 µm) using a 4×-magnification objective lens. The power of transmitted light through the hydrogel fiber was measured with a power meter. Using a sharp knife, the 1 cm long end of the fiber was cut away, and the output power was measured after each cut. This measurement was repeated at an interval of 1 cm. Glycerol-water mixtures at various glycerol concentrations were used to investigate the optical loss to surrounding media with different refractive indices. The hydrogel fiber was inserted in a plastic tube (diameter: 3 mm), and a glycerol solution was injected in the tube by using a syringe. A large-area power meter was placed at the bottom of the tube to measure the transmitted power levels before and after the injection, respectively. The measurement was completed in less than 5 min so that the swelling state of the fiber was largely unchanged from an initial pre-swelling state.

Mechanical Test of the Hydrogel Fibers: An Instron analyzer was used to measure the stress–strain curve of hydrogel fibers. The fiber was clamped with an initial distance of 5 cm and strained at a speed of 4.8 mm min⁻¹. During the measurement, an ultrasonic humidifier (Szwisechip) was used to keep the fiber moist and avoid undesirable dehydration.

Strain Sensing: A 3 µL water droplet containing dye molecules (0.01% w/v) was applied to form a sensing region of 8–10 mm in length. The sensor fiber was taped down onto a pair of parallel mounts with a width of 5 mm and stretched by using a translation stage (Thorlabs, 10 µm resolution), and the rest of fibers including sensing regions were hanging in the air. An ultrasonic humidifier was used to keep the fiber moist. The attenuation spectra were measured by using a white light source (Fisher Scientific) and a spectrometer (Thorlabs, CCS100).

Supporting Information

Supporting Information is available from the Wiley Online Library or from the author.

Acknowledgements

[1] K. Y. Lee, D. J. Mooney, *Chem. Rev.* **2001**, *101*, 1869.
[2] T. R. Hoarea, D. S. Kohane, *Polymer* **2008**, *49*, 1993.
[3] J. Madsen, S. P. Armes, K. Bertal, H. Lomas, S. MacNeil, A. L. Lewis, *Biomacromolecules* **2008**, *9*, 2265.
[4] M. Choi, M. Humar, S. Kim, S. Yun, *Adv. Mater.* **2015**, *27*, 4081.
[5] M. Choi, J. W. Choi, S. Kim, S. Nizamoglu, S. K. Hahn, S. H. Yun, *Nat. Photonics* **2013**, *7*, 987.
[6] J. P. Monteiro, S. M. Predabon, C. T. P. Silva, E. Radovanovic, E. M. Girotto, *J. Appl. Polym. Sci.* **2015**, *132*, 42449.
[7] M. C. Darnell, J. Sun, M. Mehta, C. Johnson, P. R. Arany, Z. Suo, D. J. Mooney, *Biomaterials* **2013**, *34*, 8042.
[8] S. Lin, H. Yuk, T. Zhang, G. A. Parada, H. Koo, C. Yu, X. Zhao, *Adv. Mater.* **2015**, *28*, 4497.
[9] X. Zhao, *Soft Matter* **2014**, *10*, 672.
[10] Y. Tanaka, J. P. Gong, Y. Osada, *Prog. Polym. Sci.* **2005**, *30*, 1.
[11] J. Sun, X. Zhao, W. R. K. Illeperuma, O. Chaudhuri, K. H. Oh, D. J. Mooney, J. J. Vlassak, Z. Suo, *Nature* **2012**, *489*, 133.
[12] H. Yuk, T. Zhang, S. Lin, G. A. Parada, X. Zhao, *Nat. Mater.* **2016**, *15*, 190.
[13] C. H. Yang, M. X. Wang, H. Haider, J. H. Yang, J. Sun, Y. M. Chen, J. Zhou, Z. Suo, *ACS Appl. Mater. Interfaces* **2013**, *5*, 10418.
[14] C. Cha, E. Antoniadou, M. Lee, J. H. Jeong, W. W. Ahmed, T. A. Saif, S. A. Boppart, H. Kong, *Angew. Chem. Int. Ed.* **2013**, *52*, 6949.
[15] M. B. Applegate, G. Perotto, D. L. Kaplan, F. G. Omenetto, *Biomed. Opt. Express* **2015**, *6*, 4221.
[16] S. L. Jacques, *Phys. Med. Biol.* **2013**, *58*, R37.
[17] A. I. Lvovsky, in *Encyclopedia of Optical Engineering* (Ed: R. G. Driggers), Taylor and Francis, New York **2013**.
[18] M. Y. Kizilay, O. Okay, *Polymer* **2003**, *44*, 5239.
[19] J. A. Rogers, T. Someya, Y. Huang, *Science* **2010**, *327*, 1603.
[20] C. Pang, G. Lee, T. Kim, S. M. Kim, H. N. Kim, S. Ahn, K. Suh, *Nat. Mater.* **2012**, *11*, 795.
[21] W. Gao, S. Emaminejad, H. Y. Y. Nyein, S. Challa, K. Chen, A. Peck, H. M. Fahad, H. Ota, Hi. Shiraki, D. Kiriya, D. Lien, G. A. Brooks, R. W. Davis, A. Javey, *Nature* **2016**, *529*, 509.
[22] T. Yamada, Y. Hayamizu, Y. Yamamoto, Y. Yomogida, A. Izadi-Najafabadi, D. N. Futaba, K. Hata, *Nat. Nanotechnol.* **2011**, *6*, 296.
[23] D. J. Lipomi, M. Vosgueritchian, B. C.-K. Tee, S. L. Hellstrom, J. A. Lee, C. H. Fox, Z. Bao, *Nat. Nanotechnol.* **2011**, *6*, 788.
[24] C. Milgroma, A. Finestonec, A. Hameld, V. Mandesd, D. Burre, N. Sharkeyd, *J. Biomech.* **2008**, *30*, 104.
[25] L. Cai, L. Song, P. Luan, Q. Zhang, N. Zhang, Q. Gao, D. Zhao, X. Zhang, M. Tu, F. Yang, W. Zhou, Q. Fan, J. Luo, W. Zhou, P. M. Ajayan, S. Xie, *Sci. Rep.* **2013**, *3*, 3048.
[26] H. Ko, J. Lee, B. E. Schubert, Y. Chueh, P. W. Leu, R. S. Fearing, A. Javey, *Nano Lett.* **2009**, *9*, 2054.
[27] C. Cochrane, V. Koncar, M. Lewandowski, C. Dufour, *Sensors* **2007**, *7*, 473.
[28] P. Roriz, L. Carvalho, O. Frazão, J. L. Santos, J. A. Simões, *J. Biomech.* **2014**, *47*, 1251.
[29] T. Fresvig, P. Ludvigsen, H. Steen, O. Reikeras, *Med. Eng. Phys.* **2008**, *30*, 104.
[30] A. Othonos, *Rev. Sci. Instrum.* **1997**, *8*, 4309.
[31] S. Nizamoglu, M. C. Gather, S. H. Yun, *Adv. Mater.* **2013**, *25*, 5943.
[32] R. C. S. B. Allil, M. M. Werneck, *IEEE Trans. Instrum. Meas.* **2011**, *60*, 2118.
[33] T. Takigawa, Y. Morino, K. Urayama, T. Masuda, *Polym. Gels Networks* **1996**, *4*, 1.
[34] C. X. Wang, C. Cowen, Z. Zhang, C. R. Thomas, *Chem. Eng. Sci.* **2005**, *60*, 6649.
[35] B. Stuart, *Modern Infrared Spectroscopy*, Wiley, Hoboken, NJ, USA **1996**, Ch. 3.
[36] R. Lansford, G. Bearman, S. E. Fraser, *J. Biomed. Opt.* **2011**, *6*, 311.
[37] M. Wang, Y. Guo, R. A. Hayes, D. Liu, D. J. Broer, G. Zhou, *Materials* **2016**, *9*, 250.